



Atomistic modeling of finite-temperature properties of crystalline β -SiC

II. Thermal conductivity and effects of point defects

Ju Li, Lisa Porter¹, Sidney Yip^{*}

Department of Nuclear Engineering, Massachusetts Institute of Technology, Cambridge, MA 02139-4307, USA

Received 20 October 1997; accepted 2 February 1998

Abstract

In this, the second part of a theoretical study of the thermal properties of crystalline β -SiC, the thermal conductivity is calculated by using molecular dynamics simulation to evaluate directly the heat current correlation function and thus, obtain the conductivity through the Green–Kubo expression in linear response theory. Adopting the same empirical potential model and the temperature scaling method as in part one, we predict absolute conductivity values for a perfect crystal which are in satisfactory agreement with available data, except in the low-temperature region (below 400 K) where quantum effects become dominant. The effects of carbon and silicon vacancies and antisite defects are studied by introducing a single defect into the simulation cell, allowing the atomic configuration to relax, and then performing heat capacity, thermal expansion and conductivity calculations. We find that the heat capacity and thermal expansion coefficient are affected very little by point defects even at a high concentration of 0.5%. On the other hand, the thermal conductivity is observed to degrade markedly as a result of the greatly enhanced decay of the heat current correlation, clearly attributable to the dominant mechanism of defect scattering of phonons. The defect simulations also reveal that the conductivity becomes essentially temperature independent. Both characteristics appear to have correspondence with observations on conductivity behavior in neutron-irradiated specimens. © 1998 Elsevier Science B.V. All rights reserved.

1. Introduction

Since Debye first considered the calculation of the thermal conductivity κ of a non-metallic crystal in 1914, simple expressions suitable for making qualitative estimates have been derived in terms of physical properties such as the Debye temperature and the Gruneisen parameter, or alternatively, in terms of the phonon mean lifetime and the specific heat (Slack [1]). For quantitative calculations, the traditional approach has been to consider phonon interactions explicitly but invoke continuum approximations to make the calculations tractable (Leibfried [2],

Ziman [3], Srivastava [4]). Recently, a calculation of the three-phonon scattering contribution to κ , which considers directly the discrete nature of the crystal lattice has been reported (Omini and Sparavigna [5]), and even extended to account for the actual structure of the Brillouin zone (Omini and Sparavigna [6]). While it is significant that pair interatomic potentials yielded numerical results that compare well with measurements on argon and krypton, it is also clear that calculation of lattice contribution to thermal resistance based on explicit account of phonon interactions will entail formidable analysis (Ziman [3], Berman [7], Omini and Sparavigna [5,6]).

In contrast to the lattice dynamical approach, an alternative method of calculating κ is available through the Green–Kubo formalism of time correlation functions in statistical mechanics (McQuarrie [8], Boon and Yip [9]), or equivalently, linear response theory. In this method which is formally exact, each transport coefficient is given by the

^{*} Corresponding author. E-mail: syip@mit.edu.

¹ Present address: Institute for Defense Analyses, Alexandria, VA 22311, USA.

integral of a time-dependent correlation of an appropriate microscopic flux. The entire dynamics of the system is expressed through a time correlation function, a well defined quantity that invokes no assumption concerning the physical state of the medium. From the computational standpoint, the fact that such correlation functions are amenable to molecular dynamics simulation (Rahman [10], Alder et al. [11]) is a significant advantage. Since molecular dynamics simulations require as input only the interatomic interaction, once the interatomic potential for the system of interest can be established, the calculation of κ , and of all other physical properties of the medium for that matter, in effect amounts to a prediction. Applications of the Green–Kubo method to determine transport coefficients in liquids are now quite routine (Gass et al. [12], Hansen and McDonald [13]). Studies of thermal conductivity in solids also have been reported (Ladd et al. [14], Lee et al. [15], Richardson and Clancy [16], Kitagawa et al. [17]); however, studies which address materials science issues are still rather limited (Lee et al. [15], Richardson and Clancy [16], Kitagawa et al. [17]).

In this paper, we continue the study of thermal properties of β -SiC through molecular dynamics simulation and the use of a many-body interatomic potential model (Tersoff, [18–20]) which emphasizes the bond order nature of covalent solids. In an earlier paper (Porter et al. [21]), which we hereafter refer to as Paper I, we have shown that this model provides a rather satisfactory description of the lattice vibrations, heat capacities and thermal expansion of the perfect crystal. Here we will apply the equilibrium correlation function method in conjunction with molecular dynamics simulation to determine the thermal conductivity κ over a wide temperature range. We also consider the presence of vacancy and antisite defects and their effects on the various physical properties including κ .

Our results on the perfect crystal extend over the temperature range 300–1600 K. Comparison with available data (Taylor et al. [22], Senor et al. [23]) shows satisfactory agreement above 500 K. This we regard as primary validation of our study of thermal conductivity in β -SiC, based on the combination of the Tersoff bond-order potential model and the Green–Kubo method of transport coefficient calculation through molecular dynamics simulation. In the low temperature regime (below about 400 K), there are issues concerning system size effects, poor statistics in averaging over initial conditions, and the breakdown of the method of temperature scaling used to apply quantum corrections, which still require further investigation. On the experimental side, there are also issues of sensitivity to sample sizes and microstructural details which introduce uncertainties in any comparisons with present calculations.

On the defect studies, our results show that at concentrations as high as 0.5%, the point defects considered have practically no effect on the heat capacity and expansivity. On the other hand, their effects on κ at 0.5% concentra-

tion are a pronounced reduction, up to one order of magnitude, along with an essentially total loss of temperature dependence. Interestingly, they bear a semi-quantitative correspondence with experimental observations on SiC specimens which have undergone significant irradiation (Price [24], Senor et al. [23]).

2. Methodology

The definition of κ is based on a phenomenological equation for the macroscopic heat current,

$$J^q = -\kappa \nabla T; \quad (1)$$

here κ should be a 3×3 tensor, if Eq. (1) is to hold. For crystals with point symmetry higher than T_d , such as β -SiC, κ is a scalar matrix.

The method we will use in this work to calculate the thermal conductivity tensor κ is based on the formalism of time-correlation functions where transport coefficients of a system of N interacting atoms are given by the time integrals of appropriate equilibrium correlation functions (McQuarrie [8], Boon and Yip [9]). In the case of the thermal conductivity, the correlation function that is needed is the heat current correlation,

$$\kappa = \frac{1}{k_B T^2 \Omega} \int_0^\infty d\tau \langle J^q(0) J^q(\tau) \rangle, \quad (2)$$

where

$$J^q = \sum_i \left((E_i - h) v_i + \sum_{j \neq i} r_{ij} \left(\frac{\partial E_i}{\partial r_j} v_j \right) \right) \quad (3)$$

is the instantaneous *microscopic* heat current, E_i is the internal energy of atom i with velocity v_i , h is the average enthalpy per atom, and $r_{ij} = r_i - r_j$. The first term in Eq. (3) represents the convective contribution. The second term describes energy transport through interatomic interactions. The angular brackets denote an average over the canonical ensemble. Eq. (2), along with similar expressions for the shear and bulk viscosities, and the self-diffusion coefficient, are known as Green–Kubo formulas (Green [25], Kubo [26]). They are consequences of the fluctuation–dissipation theorem which relates the linear dissipative response to external perturbations to the spontaneous fluctuations in thermal equilibrium (Kubo [26]).

We evaluate the heat current correlation function $\langle J^q(0) J^q(\tau) \rangle$ by molecular dynamics simulation. Classical Newtonian equations of motion for the N -particle system are solved numerically to give the atomic positions and velocities as the system evolves in time. These coordinates are used to compute $J^q(t)$, the instantaneous heat current [see Eq. (3)]. The data are first saved on disk, then

at the end of the simulation $\langle \mathbf{J}^q(0)\mathbf{J}^q(\tau) \rangle$ is calculated using fast Fourier transforms and the spectral method,

$$\langle \mathbf{J}^q(0)\mathbf{J}^q(\tau) \rangle = \frac{1}{2\pi T} \int_{-\infty}^{+\infty} \mathbf{J}^{q*}(\omega) \mathbf{J}^q(\omega) \exp(-i\omega\tau) d\omega, \quad (4)$$

where

$$\mathbf{J}^q(\omega) = \int_0^T \mathbf{J}^q(t) e^{+i\omega t} dt. \quad (5)$$

A flowchart of the method is given in Fig. 1. Once the correlation function is determined, its time integral, computed numerically, gives the thermal conductivity (cf. Eq. (2)). This is the approach we use, because we think the correlation function is more intuitive and easier to use in time (τ) coordinate. Alternatively, we can determine κ_{ij} by taking the $\omega \rightarrow 0$ limit of $J_i^q(\omega)J_j^{q*}(\omega)/2T$, where $J_i^q(\omega)$ is the frequency spectrum of the i th-component heat current (Lee et al. [15]). In practice, this limit should be taken with some care (Li and Yip [27]), as we only have data in a finite period.

We have chosen the spectral method because, in dealing with ‘stiff’ solids like β -SiC, very long runs are required to obtain meaningful results of $\langle \mathbf{J}^q(0)\mathbf{J}^q(\tau) \rangle$. For instance, a minimal simulation run for β -SiC crystal at 760 K takes 1300 ps; with a stepsize of 0.3 fs to ensure numerical accuracy, this translates to a simulation run of $M = 4 \times 10^6$ timesteps. On the other hand, correlation in the heat current can extend to longer than 100 ps, which corresponds to 10^5 timesteps. If we directly calculate the correlation function by averaging over products $J_i^q(t)J_j^q(t + \tau)$, we face multiplication operations on the order of 10^{11} . The computational task is significantly reduced if we instead use the spectral method of Eqs. (4) and (5); the calculation then involves only $\mathcal{O}(M \log M)$ multiplications.

In applying this procedure using the Tersoff interatomic potential model (Paper I) which describes β -SiC in terms of bond-order many-body interactions, one needs to specify how the potential energy is divided among the interacting atoms. Since there is no unique way of partitioning, we

adopt the simple procedure of dividing the potential energy equally between the bonding atoms i and j and giving nothing to the neighboring atoms k , which constitute the local environment. It has been suggested that for short-range interactions (as in the present case), the details of the division are not important (Lee et al. [15]) because temperature gradients in applications have macroscopic length scales. Accordingly, we set $W_{ij} = V_{ij}/2$ and write the contribution to J^q from $\Delta E_i = W_{ij}/2$ and $\Delta E_j = W_{ij}/2$ as

$$\mathbf{r}_{ij} \left(\frac{1}{2} \frac{\partial W_{ij}}{\partial \mathbf{r}_j} \mathbf{v}_j \right) + \mathbf{r}_{ik} \left(\frac{1}{2} \frac{\partial W_{ij}}{\partial \mathbf{r}_k} \mathbf{v}_k \right) \quad (6)$$

and

$$\mathbf{r}_{ji} \left(\frac{1}{2} \frac{\partial W_{ij}}{\partial \mathbf{r}_i} \mathbf{v}_i \right) + \mathbf{r}_{jk} \left(\frac{1}{2} \frac{\partial W_{ij}}{\partial \mathbf{r}_k} \mathbf{v}_k \right), \quad (7)$$

respectively. Adding these two contributions gives

$$\mathbf{J}_{ijk}^q = \frac{1}{2} \mathbf{r}_{ji} (\Delta \mathbf{F}_j \cdot \mathbf{v}_j - \Delta \mathbf{F}_i \cdot \mathbf{v}_i) - \frac{1}{2} (\mathbf{r}_{jk} - \mathbf{r}_{ki}) (\Delta \mathbf{F}_k \cdot \mathbf{v}_k), \quad (8)$$

with $\Delta \mathbf{F}_\alpha = -(\partial W_{ij})/(\partial \mathbf{r}_\alpha)$, $\alpha = i, j, k$, are the force contributions to atom α from the ijk triplet (and not the net force on each atom). The total heat current is the sum of all of these three-body contributions, plus the convection part [cf. Eq. (3)].

Because our molecular dynamics simulation is classical, we need to apply certain quantum corrections for neglecting discrete energy levels and zero-point vibrations, which are important at low temperatures. As we have discussed in Paper I, a temperature rescaling procedure (Wang et al. [28], Lee et al. [15]) has been found to be quite effective in correcting classical simulation results for the thermal expansion coefficient and heat capacity in comparison with experiments. In this procedure, a molecular dynamics simulation temperature T_{MD} is related to the actual temperature of measurement T ,

$$3(N-1)k_B T_{\text{MD}} = \sum_k \hbar \omega_k \left(\frac{1}{2} + \frac{1}{\exp(\hbar \omega_k/k_B T) - 1} \right), \quad (9)$$

where ω_k is the k th lattice mode eigenfrequency, and the $(N-1)$ factor accounts for the fact that the center of mass is held fixed. The idea behind this rescaling scheme is that one hopes to establish a one-to-one correspondence between the real quantum system and the classical MD simulation, such that all physical observables are the same. While this hypothesis manifestly holds for the heat capacity at low temperature, since $C_V(T) = 3(N-1)k_B(dT_{\text{MD}}(T))/(dT)$, the same cannot be said for the heat current \mathbf{J}^q . In any event, we will proceed by demanding

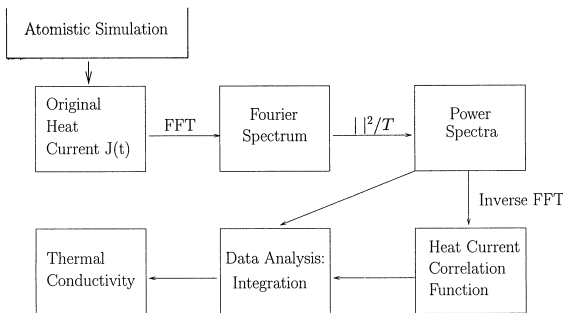


Fig. 1. Flowchart of the spectral method to calculate the thermal conductivity.

equality between simulation and experiment in the *physical* quantity of heat current J^q , then

$$J_{\text{MD}}^q = -\kappa_{\text{MD}} \nabla T_{\text{MD}} \equiv -\kappa \nabla T = J^q \quad (10)$$

which requires the conductivity calculated by classical simulation (κ_{MD}) and the observed value (κ) to have the relation

$$\kappa = \kappa_{\text{MD}} \times \left(\frac{dT_{\text{MD}}}{dT} \right). \quad (11)$$

Thus, besides rescaling the temperature, we need to multiply the κ_{MD} result of our simulation by a gradient correction, dT_{MD}/dT (Lee [15]).

There is a close relationship between Eqs. (2) and (11) and another frequently used semi-empirical formula (Ziman [3], Ladd et al. [14]),

$$\kappa = \sum_k C_V(k) \tau(k) v_g(k) v_g(k), \quad (12)$$

where an empirical parameter $\tau(k)$, the mean lifetime of each phonon-mode k , is introduced to represent the combined effect of all scattering mechanisms (phonon–phonon, phonon–defect),² which have actually been calculated by Ladd et al. (Ladd [14]) for argon-like materials. We see that instead of a phonon-specific heat capacity factor $C_V(k)$ in Eq. (12), (11) scales κ_{MD} by the overall heat capacity, as a first approximation. The decay of C_V as $T \rightarrow 0$ accounts for the vanishing of thermal conductivity at 0 K.

3. Thermal conductivity of the perfect crystal

We have made predictions of the thermal conductivity of a perfect crystal of β -SiC using the Green–Kubo method described above and the Tersoff bond-order potential model (Tersoff [19,20]) which treats β -SiC as a purely covalent solid. Molecular dynamics (MD) simulations at a series of temperatures are carried out on a cubic simulation cell containing $N = 216$ β -SiC atoms under periodic boundary conditions. The Si and C atoms interact with each other through the modified Tersoff potential (see Paper I for details of the potential model).

Newtonian equations of motion are integrated numerically with a time step size varying from 0.20 fs to 0.35 fs, depending on the system temperature. Initially, the atoms are placed in the zinc blende structure and are given velocities sampled from Maxwellian distributions. Fifty thousand to one hundred thousand time steps are allowed for equilibration, during which the simulation cell is al-

lowed to change shape and volume in response to the internal stress, while the external stress is set equal to 0 (Parrinello and Rahman [30]). Also during the equilibration phase, the atomic velocities are scaled to the desired temperature using the coupling scheme by Berendsen et al. [31] with a coupling time constant of 50 fs. After equilibration, the simulation typically continues for two to eight million steps with the simulation cell held fixed and temperature rescaling turned off. The atomic positions and velocities thus generated are the data used to evaluate the heat current correlation function.

Because β -SiC, as perfect crystal, has a high thermal conductivity, one can expect that the phonons are not easily scattered. For this reason, the initial condition (atomic velocity distribution) of a simulation run needs to be treated carefully. Different initial conditions, being different samples of a thermodynamic ensemble, may lead to very different thermal conductivity results, at least during appreciable simulation run lengths. A relatively elaborate initialization scheme has been implemented in this work. We first draw atomic velocities from a Maxwellian distribution with $\sigma_i^2 = k_B T / m_i$ (i is the atom index running from 1 to N), in three directions independently. Second, we subtract the average velocity $\bar{v} = (\sum_i^N m_i v_i) / \sum_i^N m_i$ from each atom such that the total momentum is equal to zero. Then we sum up the kinetic energies in three directions $K_\alpha = \sum_i m_i v_{i\alpha}^2 / 2$, $\alpha = 1, 2, 3$. Lastly, we scale the velocity of each atom in direction α by a factor of $\sqrt{(N-1)k_B T / K_\alpha}$ (in the harmonic approximation, the total energy is twice the kinetic energy of $k_B T / 2$), such that the same amount of kinetic energy is introduced in *each* direction. Because $\kappa_{\alpha\alpha}$ should be the same for all three directions in β -SiC, the fact that each direction has the same amount of kinetic energy tends to reduce the fluctuation if we evaluate κ , a scalar quantity, using

$$\langle J(0)J(\tau) \rangle = \sum_\alpha \langle J_\alpha^q(0)J_\alpha^q(\tau) \rangle / 3. \quad (13)$$

It can be shown that each phonon mode, be it acoustic or optical, has the same energy expectation, as it should in classical statistical mechanics.

Figs. 2–4 show the heat current correlation functions obtained at three temperatures. As with time correlation functions in general, $\langle J(0)J(\tau) \rangle$ decays over a time range which increases as the system temperature is lowered. The monotonic behavior seen indicates a diffusive conduction process which is to be expected, and it seems reasonable to regard the decay time as a convenient measure of phonon lifetime. The MD results shown are normalized to the initial or zero time values of the correlation function, which has the physical interpretation of a susceptibility. The temperature variation of this quantity, shown in Fig. 5, is seen to be rather insignificant, which means that the temperature dependence of the classical thermal conductiv-

² $v_g(k)$ is the phonon group velocity. $C_V(k)$ is the heat capacity of each phonon-mode, $C_V(k) = (\hbar^2 \omega_k^2 \exp(\hbar \omega_k / k_B T)) / (k_B T^2 (\exp(\hbar \omega_k / k_B T) - 1)^2)$.

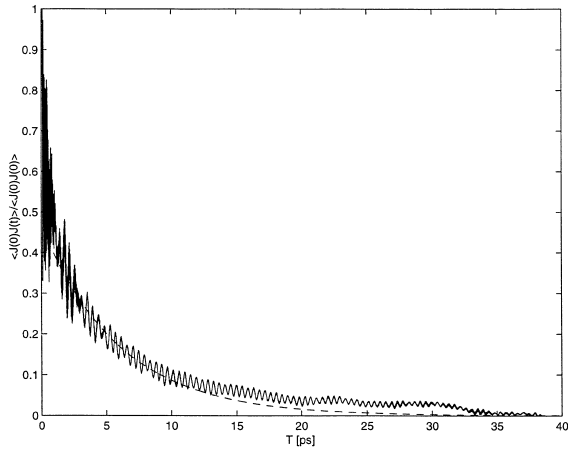


Fig. 2. Temporal decay of the equilibrium heat current correlation function for perfect β -SiC at 1400 K ($T_{MD} = 1478$ K). The dashed line is the fit to exponential decay in the range from 1 to 9 ps.

ity, κ_{MD} , depends mainly on the characteristic decay time of the heat current correlation function.

Because the simulation results invariably show fluctuations due to statistical noise, there exists some ambiguity in carrying out the time integration in Eq. (2). We have tested two ways of computing the integral, one (which we call First Dip or FD) is to integrate out to the time where the correlation function first reaches zero, while the other (Exponential Fit or EF) is to fit the correlation function to an exponential over some time range. In the latter procedure, one fits the correlation function data in the range $[\tau_1, \tau_2]$, where numerical accuracy of the results can be ensured, to an exponentially decaying curve $g \exp(-\tau/\tau_0)$. The major contribution to κ comes from the integration of the raw data between $[0, \tau_2]$, but g and τ_0 are used to determine the tail contribution between $(\tau_2, +\infty)$, which is just $g\tau_0 \exp(-\tau_2/\tau_0)$.

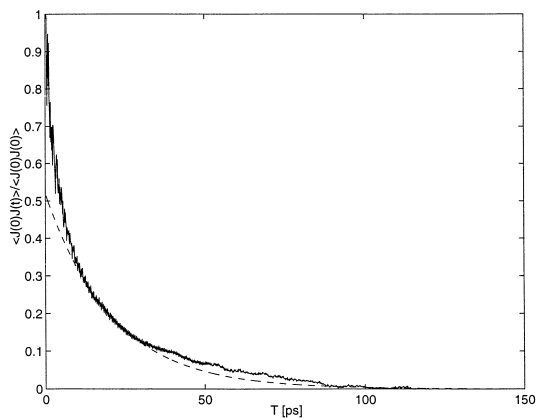


Fig. 3. Temporal decay of the equilibrium heat current correlation function for perfect β -SiC at 760 K ($T_{MD} = 885$ K). The dashed line is the fit to exponential decay in the range from 10 to 30 ps.

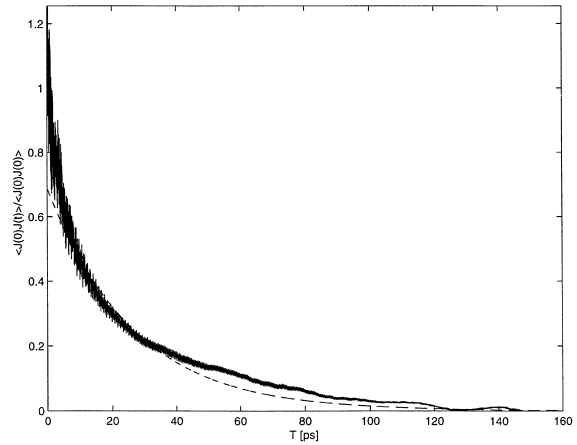


Fig. 4. Temporal decay of the equilibrium heat current correlation function for perfect β -SiC at 284 K ($T_{MD} = 552$ K). The dashed line is the fit to exponential decay in the range from 5 to 35 ps.

This method is based on the observation that the dependence of the logarithm of the raw data on τ , taken in the range of τ where simulation results are believed to be good, can be fairly well approximated as a straight line, leading us to believe that $\langle J(0)J(\tau) \rangle$ may decay asymptotically as an exponential. The only parameters that the EF method requires are τ_1 and τ_2 ; our recommended values are given in Table 1.

Usually, $\langle J(0)J(\tau) \rangle$ from carefully implemented and well-converged simulation runs will give FD and EF results close to each other, especially at high temperatures. We think that for a single minimal run, the EF result may be more accurate because the procedure acts as a filter. However, when one can do very long simulations, and many of them, the FD method will yield better results.

Table 2 gives a summary of our simulation results for perfect crystal β -SiC: the MD value of the conductivity,

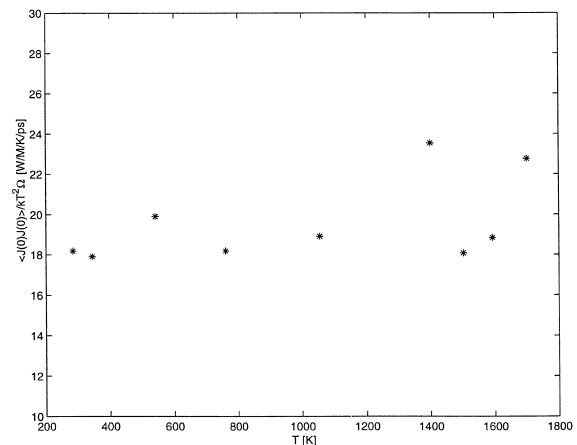


Fig. 5. Calculated $\langle J(0)^2 \rangle / k_B T^2 \Omega = \sum_{\alpha} \langle J_{\alpha}^q(0)^2 \rangle / 3k_B T^2 \Omega$ in perfect β -SiC crystal vs. temperature.

Table 1

Recommended simulation parameters for perfect crystal β -SiC thermal conductivity calculation

T (K)	Steps	Timestep (fs)	Runs	EF τ_1 (ps)	EF τ_2 (ps)
250–500	8×10^6	0.30–0.35	6–10	5.0	35.0
500–1000	4×10^6	0.25–0.30	4–6	3.5	21.0
1000–1600	4×10^6	0.20–0.25	2–4	1.0	9.0

κ_{MD} , the gradient correction factor, $(dT_{MD})/(dT)$, the corrected values of the conductivity, κ , and conductivity values interpolated from experimental data (Taylor et al. [22]). Except for the very lowest temperature value, the agreement between simulation and measurement is seen to be satisfactory. It is also somewhat remarkable that a classical simulation with two corrections, a temperature rescaling and a conductivity rescaling, is able to give semiquantitatively accurate predictions down to about a third of the Debye temperature ($\theta_D \approx 1200$ K, Senor et al. [23]). In view of the fact that the Tersoff potential model was not fitted to any thermal property, we believe this constitutes significant evidence that this bond-order potential describes adequately the anharmonic effects in SiC, which is consistent with what we have previously found in the thermal expansivity calculations (Paper I). The comparison of simulation with two sets of experimental data (Taylor et al. [22], Senor et al. [23]) is also shown in Fig. 6. The results of Senor et al. are generally lower in value; even though their samples are of high purity and are fully dense, we believe the difference between these data and those of Taylor et al. [22] is an indication of higher defect content in the former specimens.

The low temperature behavior of our simulations warrants further discussion. First, our simulations significantly

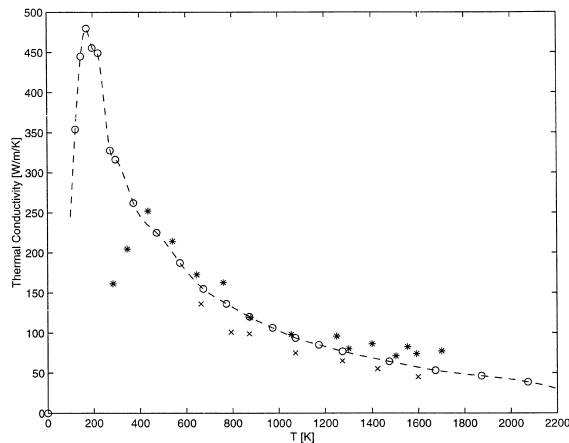


Fig. 6. Comparison of calculated thermal conductivity for perfect crystal β -SiC with experiments at various temperatures. The circles are experimental results from Taylor et al. [22], the dashed line being its spline fit. The stars are calculated results. Experimental results from Senor et al. [23] are plotted in crosses.

underpredict κ for $T < 400$ K; second, although qualitatively the same behavior in the variation of κ in the form of a sharp peak is observed both in simulation and in experimental data, the peak in the simulation result occurs at a much higher temperature than the experimental peak, whereas the agreement is quite satisfactory at higher temperatures.

There are several factors that contribute to the divergence of our simulation results from the experimental data at low temperatures. We note from Table 2 that below 400 K, there is a combined effect of a sharp drop in $(dT_{MD})/(dT)$ and a significant leveling off in the growth of κ_{MD} . The leveling off of κ_{MD} occurs in part because of the flatness of the T_{MD} vs. T curve as $T \rightarrow 0$ (see Fig. 2

Table 2

Thermal conductivity calculation for perfect SiC crystal

T (K)	T_{MD} (K)	$(dT_{MD})/(dT)$	N	Steps	Runs	κ_{MD}^a	κ^a	Experimental ^a
284	552	0.429	216	8×10^6	12	397.3	161.3	318.6
345	582	0.533	216	8×10^6	4	383.7	204.6	285.7
436	634	0.648	216	4×10^6	1	374.0	252.1	235.0
541	709	0.741	216	4×10^6	1	289.2	214.3	200.4
645	790	0.804	216	4×10^6	1	214.7	172.6	162.4
760	885	0.851	216	4×10^6	8	191.2	162.7	138.5
876	985	0.884	216	4×10^6	1	134.8	119.2	120.0
1055	1150	0.917	216	2×10^6	2	107.0	98.1	95.8
1249	1335	0.940	216	2×10^6	1	102.0	95.9	78.9
1300	1383	0.944	216	2×10^6	1	85.0	80.2	75.0
1400	1478	0.951	216	8×10^6	4	90.8	86.3	68.6
1502	1575	0.958	512	2×10^6	1	74.4	71.2	62.6
1553	1624	0.960	216	2×10^6	1	86.2	82.8	60.0
1592	1661	0.962	216	2×10^6	1	77.0	74.1	57.3
1700	1764	0.967	216	4×10^6	4	80.2	77.5	51.9

^aResults are in SI unit of W/M/K.

of Paper I). Specifically, in this temperature region, T_{MD} changes only from 634 K to 552 K as T changes from 436 K to 284 K.³ Furthermore, there is a fundamental limitation in our use of the gradient correction factor, $(dT_{\text{MD}})/(dT)$, in Eq. (11), which is easily understood when Eq. (11) is compared with the semi-empirical quantum mechanical formula for κ , Eq. (12). There, a ‘gradient correction factor’ is also present in the form of a mode-specific heat capacity. Hence, in implementing Eq. (11), we have assumed that we can replace the mode-specific heat capacity, $C_V(k, T)$, with the overall heat capacity, $C_V(T)$.

This introduces an error, because we believe that the factor $\tau(k) v_g(k) v_g(k)$ in Eq. (12) is perhaps larger at small k ($\tau(k) v_g(k) v_g(k)$ is just the product of the mean free path and the group velocity of mode k). At low temperatures, $C_V(k, T)$ is larger for small k , and therefore, the larger values of $\tau(k) v_g(k) v_g(k)$ corresponding to the longer wavelength phonons should be weighted more heavily (this is true for all $T \sim \theta_D$, but is most important as $T \rightarrow 0$). By using the overall heat capacity, we have essentially applied equal weighting to all modes, which therefore leads to an underestimation of κ at low temperatures.

In addition to the limitations to our approach discussed above, there are two computational issues, system size effect and statistical accuracy, which are natural causes for concern for simulations performed at low temperatures. It is expected that as the temperature decreases, the low frequency, and therefore long wavelength, phonons play an increasingly important role. This is true for two reasons. First, as $T \rightarrow 0$, long wavelength phonons become relatively more important than their high frequency counterparts, because their occupation numbers are larger (i.e., equipartition theorem breaks down at low temperature). Second, as discussed above, we believe that the factor $\tau(k) v_g(k) v_g(k)$ appearing in Eq. (12) will be larger for longer wavelength phonons. Because there is always a wavelength cutoff associated with a finite simulation cell, it is therefore reasonable to argue that system size effect alone will cause the thermal conductivity to be underestimated (Lee et al. [15]). On the other hand, limited studies of system size (i.e., the number of atoms, N , in the simulation cell) in rare-gas solids have shown little variation in κ with N , and it was suggested that this could be due to a cancellation effect, as newly introduced phonon modes would increase the scattering probabilities and therefore lower the lifetimes of phonons already in existence (Ladd [14]). Concerning statistical accuracy, we have

observed that our low-temperature simulations are very sensitive to the set up of initial conditions. This is not surprising from the standpoint that with the crystal becoming nearly harmonic, very long runs are needed to achieve a reasonably equilibrated phonon distribution at these temperatures. For example, a simulation run of eight million time steps, relatively long by present standards (Ladd et al. [14], Lee et al. [15], Richardson and Clancy [16], Kitagawa et al. [17]), still has an estimated error bar of 20%. Clearly then, substantially greater computational efforts will be required to obtain conductivity results below 400 K to have the same quality as those at higher temperatures.

As far as the low temperature regime of the experimental thermal conductivity is concerned, it is well known from studies of rare gas crystals that below approximately $\theta_D/4$, the data are very sensitive to the effects of specimen sizes and crystal imperfections (Gupta and Trikha [33,34]). Thus, there is uncertainty not only in our simulation results, but also in the experimental data at low temperatures.

Before leaving this section, it should be noted that the slow convergence problem encountered previously (Kitagawa et al. [17]) in the low temperature region does not occur if one uses the temperature rescaling scheme by Lee et al. [15], because T_{MD} is always appreciable. In the present case, T_{MD} is always greater than 500 K.

4. Point defects in β -SiC

As part of the present work, we consider how the presence of point defects affect the thermal properties of β -SiC. Given that a systematic study of point defect generation under irradiation conditions and their subsequent distribution in the solid is beyond the scope of our investigation, we will limit our calculations to elucidating generic effects of defect–phonon interactions in well-characterized defective lattices. Thus, we will first determine the relaxed atomic configuration when a single point defect is introduced into the simulation cell, and then apply the methods we have described in Paper I and the foregoing sections to calculate the density of states, heat capacity and thermal expansion coefficient, and the conductivity for each type of defect. Using the previous simulation cell containing $N = 216$ atoms as the natural reference system, we note that with one isolated defect in the simulation cell, the effective defect concentration is already 0.5%. This concentration level, admittedly, may not be stable against clustering and formation of extended defects such as voids and dislocation loops. With this in mind, we do not expect that our results can be directly compared with measurements on irradiated samples. On the other hand, the simulation results should provide a baseline that is useful for interpretation purposes.

³ A similar problem occurred for the MD calculations of the thermal expansion coefficient, α , at low T in Paper I. Uncertainty in α below 250 K resulted from the flatness of the T_{MD} dependence on T at low T .

4.1. Relaxed defect structures

We define the formation energy of a given point defect to be the difference in total energy between the system with the defect and the reference system (perfect crystal) which has the same number of atoms,

$$E_f = E(N_d) - \frac{E_0(N_p)}{N_p} N_d, \quad (14)$$

where $E(N_d)$ and $E_0(N_p)$ are the respective total energies, and N_p (N_d) are the number of atoms in the perfect (defect) system. This definition is necessary because for a multi-component system the chemical potential for different species cannot be compared. Eq. (14) provides a convenient basis for comparison with other studies. For the present potential model (Tersoff [19,20], Paper I), we have $E_0(N_p)/N_p = -6.386497$ eV and the equilibrium lattice constant $a_0 = 4.28533$ Å.

Static energy minimization in a 216-particle cell with periodic boundary conditions has been carried out using the conjugate gradient algorithm (Press et al. [35]). Relaxed defect configurations and E_f , under both constant volume (lattice constant = a_0) and constant pressure ($P = 0$) conditions have been obtained. As an independent check, these configurations were also relaxed by molecular dynamics under constant volume with a simple annealing procedure, and the results were found to be in complete agreement with static minimizations. Ten point defects have been studied; these include carbon and silicon vacancies (V_C and V_{Si}), carbon and silicon antisites (C_{Si} and Si_C), carbon and silicon interstitials at tetrahedral sites with four carbon (silicon) neighbors [C_{TC} (C_{TSi}) and Si_{TC} (Si_{TSi})], antisite pair (AP) defect where a nearest neighbor pair of Si and C atoms are switched, and divacancy (DI) where a nearest neighbor pair of Si and C atoms are pulled out.

We found that the relaxed defect configurations can depend sensitively on the cutoff parameters of the potential. With the nearest Si–Si separation in perfect β -SiC

crystal at 3.03 Å, Si atoms can be quite easily displaced, by virtue of local distortion, to cross into the potential cutoff of 2.7/3.0 Å and give rise to undesirable interactions between atoms, which ordinarily are second nearest neighbors and therefore should be excluded by the cutoff. The same effect could also arise from thermal motions at high temperatures (for this reason in Paper I we proposed to discard the Si–Si interactions altogether while studying the thermal properties of β -SiC crystal). While this effect on the defect formation energy is not appreciable, it does strongly disturb the particle dynamics, such as leading to unphysical high-frequency local modes in the vibrational spectrum (see next section). We have decided to modify the Si–Si and C–C cutoffs by using a unified value of 2.36/2.56 Å, which effectively blocks out second nearest neighbor Si–Si interactions. We will call this modified potential *Ters1*. For comparison, we will also give the defect formation energies obtained using the original Tersoff potential (Tersoff [19,20]) which we denote as *Ters2*.

Our results are shown in Table 3 along with a recent study (Huang et al. [36]), believed to be based on the same Tersoff model, and values from an ab initio calculation (Wang et al. [37]). The P or V inside the bracket denotes whether it is a constant pressure or constant volume minimization.

In comparing *Ters2(V)* with the recently published results (Huang et al. [36]), we find acceptable agreement in the case of vacancy defects, but significant disagreement in other defects. At present we know of no other cause of this discrepancy except that [36] possibly did not use the same set of parameters as ours.

Adding the energies of the two antisite defects, we find that *Ters1(V)* predicts 6.4 eV for generating the two defects by switching a Si atom and a C atom separated infinitely far away. If we put them side by side, the formation energy will be reduced to 3.9 eV, an indication that the two defects ‘attract’ each other, which could be interpreted as arising from a size effect where the two antisites compensate for the excess volume of each other. The formation energies for the vacancies and the diva-

Table 3
Defect formation energies (eV)

Defect	<i>Ters1(P)</i>	<i>Ters1(V)</i>	<i>Ters2(V)</i>	(V) Ref. [36]	Ab initio (V) Ref. [37]
V_C	5.41	5.41	5.5	5.2	5.9
V_{Si}	6.20	6.20	6.2	6.0	6.8
C_{Si}	-0.31	-0.27	-0.2	0.6	1.1
Si_C	6.57	6.65	8.8	5.6	7.3
C_{TC}	13.67	13.75	6.2	8.7	11.0
C_{TSi}	16.48	16.57	3.1	6.7	8.6
Si_{TSi}	19.63	19.90	20.2	14.4	15.0
Si_{TC}	14.98	15.47	19.7	10.5	14.7
AP	3.91	3.92	4.4	N/A	5.9
DI	8.71	8.71	8.7	N/A	8.1

Table 4

Excess volume (10^{-30} m^3) calculated by *Ters1(P)*

V_C	V_{Si}	C_{Si}	Si_C	C_{TC}	C_{TSi}	Si_{TSi}	Si_{TC}	AP	DI
2.68	1.85	-9.52	15.44	15.33	16.48	27.88	37.22	3.88	3.44

cancy defects agree reasonably well with the ab initio results. As for the carbon and silicon interstitials at tetrahedral sites, the disagreement shows that the Tersoff potential model is unsuitable to describe defects with large distortions.

Using constant pressure ($P = 0$) minimization, we have calculated the excess volume of each defect, defined as the change in cell volume before and after putting in the defect. They are tabulated in Table 4.

We see that except for C_{Si} antisite, all other defects cause the cell to expand. For the silicon and carbon vacancies, the surrounding atoms are found to relax outward rather than inward when the atom is removed. This is because when one bond is broken, the remaining three bonds are strengthened due to reduced screening, the same effect seen in inward relaxation of silicon surfaces.

4.2. Density of states

A fundamental characterization of the vibrational properties of a solid is its density of states (DOS), the distribution of lattice mode eigenfrequencies. In particle simulation, we built up theoretical models for real solids by stacking up infinitely many *supercells*, each containing 10^2 to 10^6 atoms, in three dimensions, to simulate the bulk behavior of a macroscopic solid which contains 10^{23} atoms. Of course, as the size of the supercell grows, and provided that the interaction potential is accurate, our theoretical model will approach the real solid. Nevertheless, even for such a ‘model solid’ with a finite-size supercell, it still can have a continuous vibrational DOS, i.e., infinitely many possible lattice modes, because although the supercell structure is duplicated spatially, the lattice mode displacements could be multiplied by a phase factor $e^{i\mathbf{k} \cdot \mathbf{R}_{LM}}$, for different supercells L and M. Here \mathbf{k} is called the ‘supercell \mathbf{k} ’. This continuous DOS information is accessible to dynamical matrix studies in \mathbf{k} -space, either by direct diagonalization, or by various acceleration schemes (Heine et al. [38], Wu et al. [39–41], Li and Yip [42]). The underlying assumption is that the harmonic approximation holds, which is true at low temperatures.

As one of the methods in modeling solid behavior, molecular dynamics has many distinctive merits such as being able to study finite temperature properties. However, the lattice modes it has access to are only a discrete set ($3(N-1)$ in number) of the infinitely many possible modes, namely, they all belong to the supercell $\mathbf{k} = 0$ (Γ -point) set. The reason is that the periodic boundary condition setup in MD not only means that atoms in one

supercell interact with atoms in adjacent supercells (‘images’ of the original supercell atoms), they are also required to move ‘in phase’, i.e., the images have exactly the same displacements as the original atom. This way only the supercell $\mathbf{k} = 0$ modes are possible, and the vibrational DOS is discrete. Note, however, that this does not mean that there are no short or long wavelength phonons in the supercell, as the supercell \mathbf{k} is usually *not* the primitive cell \mathbf{k} , in the case of perfect crystal.

In studying the perfect crystal β -SiC, we have used a 216-atom supercell (by default ‘simulation cell’ or ‘cell’ means supercell), consisting of $3 \times 3 \times 3$ cubic unit cells, each with eight atoms. Thus there should be $3 \times 215 = 645$ discrete lattice modes available to our MD simulation, which are actually 645 discrete samplings of the Brillouin zone of the β -SiC primitive cell, whose Bravais lattice is FCC and contains one Si and one C atom. The longest wavelength phonons available span the supercell, $\mathbf{k} = (2\pi)/(3a_0)(\pm i \pm j \pm k)$.

Once we put a defect in the 216-atom cell, periodicity of the primitive cells are destroyed and phonons in the original sense are no longer defined. However the supercell itself is periodic and our above discussions about the supercell still hold. The DOS $\rho(\omega)$ is defined mathematically as

$$\rho(\omega) = \sum_n \delta(\omega - \omega_n) \quad (15)$$

where ω_n ’s are the lattice vibrational eigenfrequencies. In addition to the (total) DOS, we can also define a *local* density of states, LDOS,

$$\rho_i(\omega) = \sum_n \delta(\omega - \omega_n) |\langle i|n\rangle|^2, \quad (16)$$

which not only gives frequency but also spatial information. Here $|n\rangle$ denotes the n th lattice eigenmode with eigenfrequency ω_n , and i is a local coordinate such as certain direction of displacement of a given atom. Overall there should be the relation

$$\rho(\omega) = \sum_i \rho_i(\omega). \quad (17)$$

By studying LDOS of atoms close to the defect, we can see in much better detail how the appearance of a defect influences the dynamics of the system by affecting the atoms close to it.

The first step to obtain the DOS and LDOS is to calculate the force constant matrix (see Paper I), which we have analytically derived for the Tersoff potential (Porter et al. [43]). We then assemble the \mathbf{k} -space dynamical matrix by scaling each term in the matrix with $e^{i\mathbf{k} \cdot \mathbf{R}_{ij}} / \sqrt{m_i m_j}$, which should be a positive definite Hermitian matrix for stable systems.

The conventional method to proceed then is to directly diagonalize the matrix to get the eigenmodes and eigenvalues. In Fig. 7, we show the results of direct diagonalization

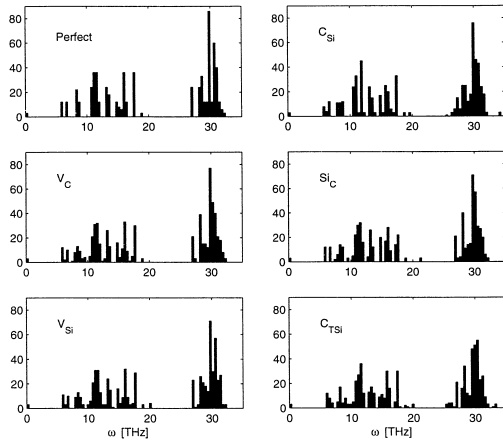


Fig. 7. Histogram of the discrete vibrational density of states (Γ -point, 0.5% defect concentration) in a 216-atom cell for perfect crystal, one carbon vacancy (V_C), one silicon vacancy (V_{Si}), one carbon antisite (C_{Si}), one silicon antisite (Si_C), and one carbon interstitial at tetrahedral silicon site (C_{TSi}), obtained by direct diagonalization method.

of the $\mathbf{k} = 0$ dynamical matrix for the atomic configuration of perfect crystal, V_C , V_{Si} , C_{Si} , Si_C and C_{TSi} interstitials, which are minimized under $Ters1(P = 0)$. These are the lattice modes that will appear in MD and hence take effect in the thermal conductivity calculations. We can see that the introduction of a point defect splits the degeneracy of the original perfect crystal spectrum, and often introduces gap modes (most obvious in Si_C and C_{TSi}) and high frequency modes (C_{Si}). These will be later shown to be local modes that are strongly associated with the few atoms surrounding the point defect and usually lie outside of the continuous spectrum of lattice vibrations. We have computed the temperature rescaling relation Eq. (9) for each defect system using the set of vibrational frequencies obtained, and the effects are found to be small. The zero-point temperatures of the various defect configurations (at 0.5% defect concentration) are listed in Table 5.

Direct diagonalization provides complete information about the system, after which we can calculate the LDOS $\rho_i(\omega)$ by summing over the normal modes of the squared amplitude of the eigenvectors at atomic coordinate i . However this process could be very time-consuming, because the computational complexity scales as N^3 , where N is the number of atoms in the supercell. So although it is possible to get continuous DOS and LDOS distribution using direct diagonalization by sampling many supercell

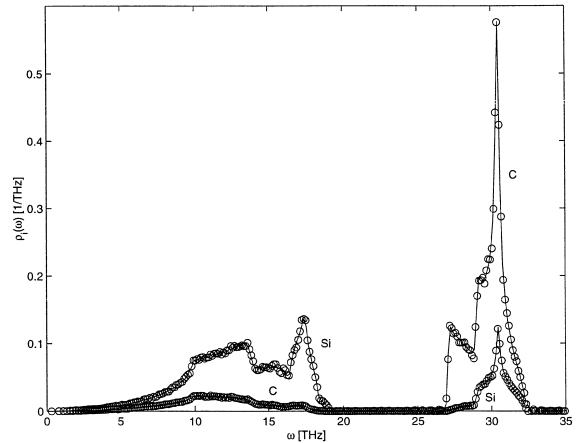


Fig. 8. LDOS of Si and C in perfect β -SiC crystal: exact phonon dispersion results by direct diagonalization (solid lines), and by a recently developed $O(N)$ method (Li and Yip [42]) (circles) in a much bigger supercell (4096 atoms).

\mathbf{k} 's, most often it is only done for the perfect crystal where we just take the smallest supercell possible—the primitive cell, and do phonon dispersion calculations. Fig. 1a in Paper I shows the DOS of perfect β -SiC crystal by directly diagonalizing 6×6 matrices in the Brillouin zone of the primitive cell (\mathbf{k} -sampling by Monte-Carlo). The corresponding LDOS for individual Si and C atoms in β -SiC are shown in Fig. 8 (because β -SiC is equivalent in x , y , z and $\rho_i(\omega)$ is the same in all directions).

Other than direct diagonalization, there are accelerated schemes to calculate the LDOS once the dynamical matrix is obtained, the most notable being the recursion method (Heine et al. [38]) and the real space Green's function method (Wu et al. [39–41]). Recently we have developed a new method called the multichannel perturbation method (Li and Yip [42]) which seems to be quite efficient; its computational complexity only scales as N , making it ideal for analyzing defect configurations relaxed in large supercells. To demonstrate the effectiveness of this new method, we re-calculate the LDOS of Si and C in perfect β -SiC crystal and compare with the phonon dispersion results. Since the method is now $O(N)$, it does not matter if we use a very large supercell, containing 4096 atoms. The results are plotted in Fig. 8 in circles.

We then apply our method to calculate the LDOS of various relaxed point defect configurations ($Ters1(P = 0)$) in the present 216-atom cell. At this system size the efficiency of our method has already surpassed that of

Table 5

Zero point vibrational energy (K) calculated by $Ters1(P = 0)$ at 0.5% defect concentration

Perfect	V_C	V_{Si}	C_{Si}	Si_C	C_{TC}	C_{TSi}	Si_{TSi}	Si_{TC}	AP	DI
512.6	510.8	510.6	514.2	508.8	508.4	508.1	505.2	510.9	511.5	509.7

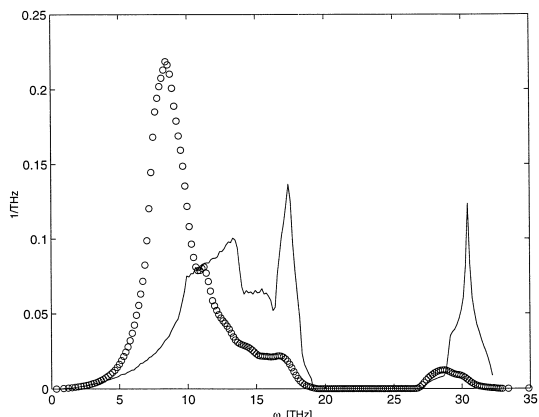


Fig. 9. $\langle 111 \rangle$ LDOS of Si atom beside V_C (circles), relaxed in a 216-atom cell ($T_{\text{ers}}(P=0)$). It is calculated by the new method (Li and Yip [42]) and by randomly sampling over 1000 supercell \mathbf{k} -points. For comparison the Si LDOS in perfect β -SiC crystal is shown in solid lines.

direct diagonalization and it is now possible to sample many ($\sim 10^3$) supercell \mathbf{k} 's. The $\langle 111 \rangle$ (debonding direction) LDOS of the nearest Si atom adjacent to a carbon vacancy is shown in Fig. 9 in circles, compared to the original perfect crystal curve in solid line. The effect is seen to be a 'mode softener'. There are no local modes induced in the spectrum.

The directionally independent (because of T_d symmetry) LDOS of the carbon interstitial atom at TSi site is shown in Fig. 10. We can clearly distinguish three peaks outside the continuous band. If we look at the discrete DOS result (Γ -point) for C_{TSi} in Fig. 7, we see that their positions correspond to certain discrete eigenvalues, however the effect is much 'magnified' in Fig. 10 because it is

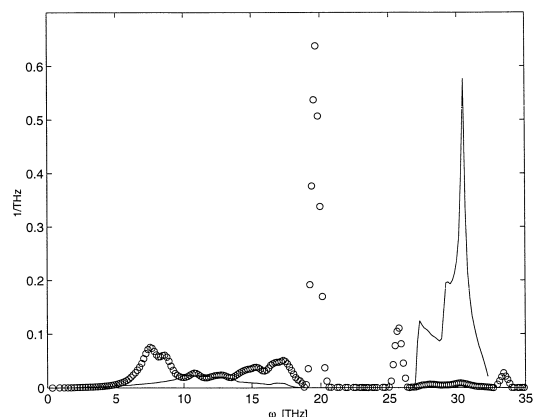


Fig. 10. LDOS of carbon interstitial atom at tetrahedral Si site, relaxed in a 216-atom cell ($T_{\text{ers}}(P=0)$). It is calculated by the new method (Li and Yip [42]) and by randomly sampling over 2000 supercell \mathbf{k} -points. For comparison the C LDOS in perfect β -SiC crystal is shown in solid lines.

the LDOS of the interstitial atom. We can see much more clearly from Fig. 10 that these modes are strongly localized around the interstitial defect instead of being propagating modes of a continuous band.

As we will discuss in the last subsection, once we put a defect in the system, the main thermal resistivity mechanism will shift from phonon-phonon collision (three-phonon process) to a phonon-defect scattering (two phonon process) mechanism. The reason that the phonons are scattered by the point defect is because of the destruction of the perfect periodicity of a perfect crystal, which adds a perturbation ΔH to the original lattice Hamiltonian H_0 , that is strongly localized around the defect. The same ΔH also alters $\rho_i(\omega)$ around the defect. Thus, in some sense the change in LDOS can be used to measure the degree of lattice distortion and hence provides some idea on how much the drop in thermal conductivity due to the defect should be.

4.3. Thermal expansion coefficient and heat capacity

The lattice dynamical method of determining the thermal expansion coefficient α which we have used in Paper I has difficulty whenever vibrational modes are introduced which do not vary smoothly with volume, thus causing the estimate of the Gruneisen parameters to be unreliable. Since the MD method does not suffer from this effect, we have used it exclusively in determining α . The results are shown in Fig. 11. As in the case of perfect crystal, all second-neighbor Si-Si interactions are turned off. It can be seen from our results that point defects have a negligible effect on the thermal expansion coefficient.

For the heat capacity, the lattice dynamical approach remains useful. Fig. 12 shows that here too the point defects have essentially no effect. The implication is that the low-frequency portion of the density of states are effectively unaltered by the point defect, as one could have

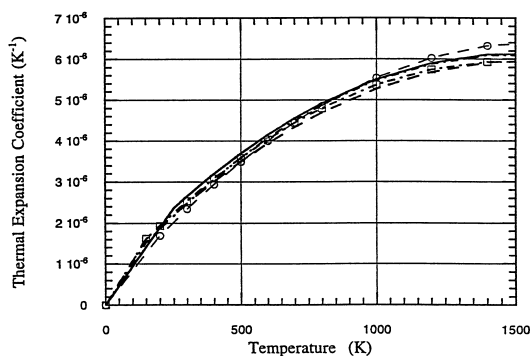


Fig. 11. Temperature dependence of thermal expansion coefficient for the perfect crystal (solid line), one carbon vacancy (dashed line), one silicon vacancy (dashed line with circles), one carbon antisite (dashed-dotted line), and one silicon antisite (dashed-dotted line with squares), in 216-atom cell.

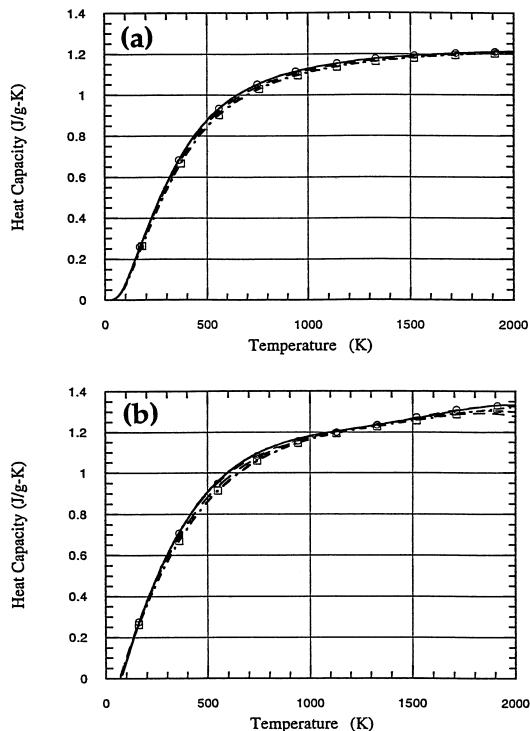


Fig. 12. Temperature dependence of the heat capacity [(a) C_V (b) C_P] for the perfect crystal (solid line), one carbon vacancy (dashed line), one silicon vacancy (dashed line with circles), one carbon antisite (dashed-dotted line), and one silicon antisite (dashed-dotted line with squares), in 216-atom cell.

discerned from Fig. 7. Our results are consistent with the insensitivity to minor constituents which has been observed in comparisons between calculated specific heat C_P values and literature data on relatively low-impurity samples, typically 95% SiC (Senor et al. [23]). Moreover, attempts to calculate specific heats using the Debye model for various SiC-based composites containing differing amounts of impurities gave virtually indistinguishable results (Senor et al. [23]).

4.4. Effects on thermal conductivity

We have carried out thermal conductivity calculations using the relaxed atomic configurations ($Ters1(P=0)$) with one point defect in the 216-atom cell. Here we report the results for V_C , V_{Si} , C_{Si} , Si_C , and Si_{TC} . Figs. 13 and 14 show the heat current autocorrelation functions $\langle J(0)J(\tau) \rangle$ for a system with one V_C at 436 K and 1592 K, along with corresponding results for the perfect crystal. The most striking feature is the much more rapid time decay of the correlation functions in the presence of a point defect. This illustrates clearly and directly the effect of defect-phonon scattering (two-phonon) mechanism, in contrast to the three-phonon process in phonon-phonon scattering, which

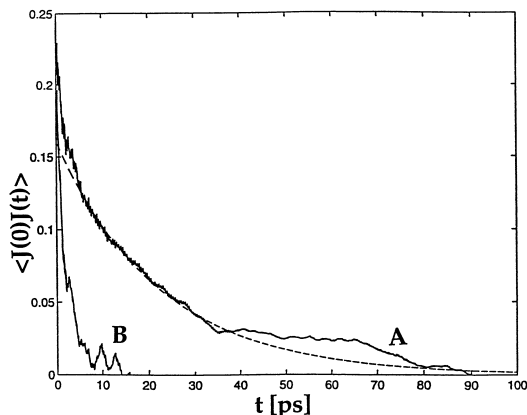


Fig. 13. Temporal decay of the equilibrium heat current autocorrelation function for β -SiC at 436 K ($T_{MD} = 634$ K), for (A) perfect crystal and for (B) with one carbon vacancy, in a 216-atom cell. The dashed line is the fit to exponential decay from 3 to 21 ps.

is the major thermal resistivity mechanism in perfect crystal. In terms of the phonon lifetime τ , these two contributions may be combined by writing

$$\frac{1}{\tau} = \frac{1}{\tau_{\text{phonon-defect}}} + \frac{1}{\tau_{\text{phonon-phonon}}}, \quad (18)$$

where $\tau_{\text{phonon-defect}}$ and $\tau_{\text{phonon-phonon}}$ are the phonon lifetimes if only either mechanism is present. We found that the point defects cause no significant changes in $\langle J(0)^2 \rangle$.

Tables 6–10 list the point defect thermal conductivity results we have obtained, also summarized in Fig. 15, which show the strong conductivity degradation effects induced by point defects. Moreover, it should be noticed from these results that the conductivity of a defected crystal, for the different defects examined, shows essentially no variation with temperature.

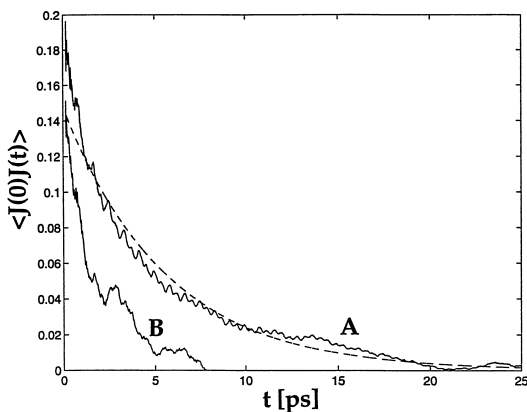


Fig. 14. Temporal decay of the equilibrium heat current autocorrelation function for β -SiC at 1592 K ($T_{MD} = 1661$ K), for (A) perfect crystal and for (B) with one carbon vacancy, in a 216-atom cell. The dashed line is the fit to exponential decay from 1 to 9 ps.

Table 6
Thermal conductivity calculation for C vacancy (0.5%)

T (K)	1578	1290	877	620	436
$\kappa(T)$ (W/M/K)	33.4	35.3	34.4	44.3	31.2

Table 7
Thermal conductivity calculation for Si vacancy (0.5%)

T (K)	1597	1316	878	624	438
$\kappa(T)$ (W/M/K)	20.0	21.3	25.9	23.2	19.8

Table 8
Thermal conductivity calculation for C antisite (0.5%)

T (K)	1652	1325	891	632	436
$\kappa(T)$ (W/M/K)	24.0	20.8	32.1	20.0	23.7

Table 9
Thermal conductivity calculation for Si antisite (0.5%)

T (K)	1305	882	649
$\kappa(T)$ (W/M/K)	20.4	14.4	15.3

Table 10
Thermal conductivity for Si interstitial at T_C site (0.5%)

T (K)	1600	1299	875	646
$\kappa(T)$ (W/M/K)	14.9	17.3	15.2	14.5

Both the degradation effect and the loss of temperature sensitivity are well documented behavior observed in conductivity measurements on irradiated specimens (Price [24], Rohde [44], Senor et al. [23]). We regard this correspondence between simulation results and irradiation data as a confirmation of the validity of the simulation; on the other hand, it is also important to recognize a significant difference exists in the defect microstructure between our simulation and the irradiation experiments. Whereas in the simulation the point defect remains as an isolated defect at the same concentration throughout the entire range of temperatures studied, the defect microstructure in the actual irradiated specimens can be expected to vary appreciably with temperature. For a high defect concentration of 0.5%, defect aggregation in the form of first self-interstitial clusters and then void formation will occur as the temperature increases, particularly in the elevated range above 1200 K. The fact that in spite of this difference simulation and experiments show the same behavior suggests that the detrimental effects of crystal defects on thermal conduction will saturate; once this occurs how the defects are

distributed then no longer matters. We therefore believe that relative to physical situations where a significant fraction of the defects are in aggregate form, the present simulation of well separated point defects can be regarded as providing the maximum effect on a per defect basis.

We have shown that the thermal conductivity of β -SiC can be calculated by combining the statistical mechanical formalism of linear response theory with molecular dynamics simulation. Although this approach has been applied previously (Ladd et al. [14], Lee et al. [15], Kitagawa et al. [17]), our work can be said to be more comprehensive and definitive in demonstrating the utility, as well as certain limitations, of the method. The findings we have presented in this two-part series should make it clear that molecular dynamics simulation indeed provides a practical and general means for determining the thermal properties of condensed matter, so long as a sufficiently realistic interatomic potential model is known for the system of interest. In terms of developing a mechanistic understanding of the heat conduction process, the accessibility to the heat current correlation function appears to be a significant advantage of the Green–Kubo approach, relative to direct calculations of the thermal conductivity based on phonon interactions.

The accuracy of the simulation results, obtained using a well-known empirical many-body potential model developed first for Si and then adapted to SiC (Tersoff [19,20]), is best brought out by comparison with experiments. Since one can improve upon the potential model by incorporating some explicit electronic-structure effects, such as in the tight-binding approximation, it remains to be seen whether better agreement with experiments can be obtained. Even without such improvements, our results for the perfect crystal and various point defects are sufficiently encourag-

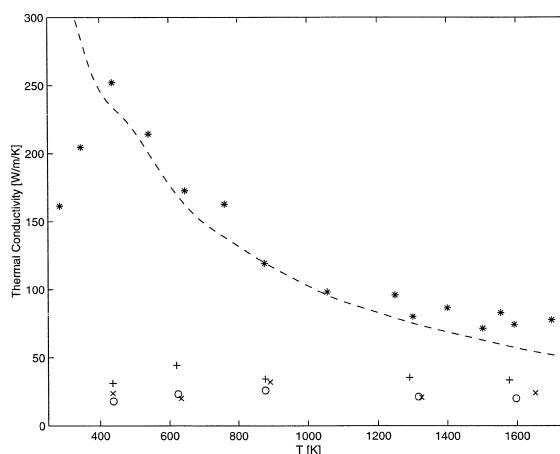


Fig. 15. Thermal conductivity as a function of temperature. Experimental values for perfect crystal are plotted in dash line. Results from calculations: perfect crystal (*), 0.5% concentration of carbon vacancy (+), 0.5% concentration of carbon antisite (x), 0.5% concentration of silicon vacancy (o).

ing to indicate that extension of the present study to other polymorphs of SiC, as well as to extended defects such as grain boundaries, dislocations, and stacking faults will be of value.

Acknowledgements

The development of the molecular dynamics code using the Tersoff potential was supported in part by AFOSR Grant No. F49620-96-1-0447. Acknowledgment is also made to the donors of The Petroleum Research Fund, administered by the ACS, for early support of J.L.

References

- [1] G.A. Slack, *Solid State Phys.* 34 (1979) 1.
- [2] G. Leibfried, in: S. Flügge (Ed.), *Handbuch der Physik*, Vol. 7, Part 1, Springer, Berlin, 1955, p. 290.
- [3] J. Ziman, *Electrons and Phonons: The Theory of Transport Phenomena in Solids*, Clarendon, Oxford, 1960.
- [4] G.P. Srivastava, *The Physics of Phonons*, Adam Hilger, Bristol, 1990.
- [5] M. Omini, A. Sparavigna, *Philos. Mag.* B 68 (1993) 767.
- [6] M. Omini, A. Sparavigna, *Phys. Rev. B* 53 (1996) 9064.
- [7] R. Berman, *Thermal Conduction in Solids*, Clarendon, Oxford, 1976.
- [8] D.A. McQuarrie, *Statistical Mechanics*, Harper and Row, New York, 1973.
- [9] J.-P. Boon, S. Yip, *Molecular Hydrodynamics*, Dover, New York, 1990.
- [10] A. Rahman, *Phys. Rev.* 159 (1967) 98.
- [11] B.J. Alder, D.M. Gass, T.E. Wainwright, *J. Chem. Phys.* 53 (1970) 3813.
- [12] D.M. Gass, B.J. Alder, T.E. Wainwright, *J. Phys. Chem. Solids* 32 (1971) 1797.
- [13] J.P. Hansen, I.R. McDonald, *Theory of Simple Liquids*, 2nd edn., Academic Press, London, 1986.
- [14] A.J.C. Ladd, W. Moran, W.G. Hoover, *Phys. Rev. B* 34 (1986) 5058.
- [15] Y.H. Lee, R. Biswas, C.M. Soukoulis, C.Z. Wang, C.T. Chan, K.M. Ho, *Phys. Rev. B* 43 (1991) 6573.
- [16] C.F. Richardson, P. Clancy, *Phys. Rev. B* 45 (1992) 12260.
- [17] H. Kitagawa, Y. Shibutani, S. Ogata, *Modell. Simul. Mater. Sci. Eng.* 3 (1995) 521.
- [18] J. Tersoff, *Phys. Rev. B* 39 (1989) 5566.
- [19] J. Tersoff, *Phys. Rev. Lett.* 64 (1990) 1757.
- [20] J. Tersoff, *Phys. Rev. B* 49 (1994) 16349.
- [21] L.J. Porter, J. Li, S. Yip, *J. Nucl. Mater.* 246 (1997) 53.
- [22] R.E. Taylor, H. Groot, J. Ferrier, *Thermophysical Properties of CVD SiC*, TRPL 1336, Thermophysical Properties Research Laboratory Report, School of Mechanical Engineering, Purdue University, November 1993.
- [23] D.J. Senior, G.E. Youngblood, C.E. Moore, D.J. Trimble, G.A. Newsome, J.J. Woods, *Fusion Technol.* 30 (1996) 943.
- [24] R.J. Price, *J. Nucl. Mater.* 46 (1973) 268.
- [25] M.S. Green, *J. Chem. Phys.* 22 (1954) 398.
- [26] R. Kubo, *Rep. Prog. Phys.* 29 (1986) 255.
- [27] J. Li, S. Yip, to be published.
- [28] C.Z. Wang, C.T. Chan, K.M. Ho, *Phys. Rev. B* 42 (1990) 276.
- [30] M. Parrinello, A. Rahman, *J. Appl. Phys.* 52 (1981) 7182.
- [31] H.J.C. Berendsen, J.P.M. Postma, W.F. van Gunsteren, A. DiNola, J.R. Haak, *J. Chem. Phys.* 81 (1984) 3684.
- [33] L.J. Gupta, S.K. Trikha, *Phys. Status Solidi B* 80 (1977) 353.
- [34] L.J. Gupta, S.K. Trikha, *Phys. Status Solidi B* 84 (1977) K95.
- [35] W.H. Press, S.A. Teukolsky, W.T. Vetterling, B.P. Flannery, *Numerical Recipes in C—the Art of Scientific Computing*, Cambridge Univ., London, 1992.
- [36] H. Huang, N.M. Ghoniem, J.K. Wong, M.I. Baskes, *Modell. Sim. Mater. Sci. Eng.* 3 (1995) 615.
- [37] C. Wang, J. Bernholc, R. Davis, *Phys. Rev. B* 38 (1988) 12752.
- [38] V. Heine, R. Haydock, M.J. Kelly, in: *Solid State Phys.*, Vol. 16, Academic Press, New York, NY, 1980.
- [39] S.Y. Wu, Z.L. Xie, N. Potoczak, *Phys. Rev. B* 48 (1993) 14826.
- [40] S.Y. Wu, J.A. Cocks, C.S. Jayanthi, *Phys. Rev. B* 49 (1994) 7959.
- [41] S.Y. Wu, C.S. Jayanthi, *Int. J. Mod. Phys.* 9 (1995) 869.
- [42] J. Li, S. Yip, *Phys. Rev. B* 56 (1997) 3524.
- [43] L.J. Porter, S. Yip, M. Yamaguchi, H. Kaburaki, M. Tang, *J. Appl. Phys.* 81 (1997) 96.
- [44] M. Rohde, *J. Nucl. Mater.* 182 (1991) 87.